SOLID-STATE PHYSICS

Quantum oscillations of electrical resistivity in an insulator

Z. Xiang[1], Y. Kasahara[2], T. Asaba[1], B. Lawson[1,3], C. Tinsman[1], Lu Chen[1], K. Sugimoto[4], S. Kawaguchi[4], Y. Sato[2], G. Li[1], S. Yao[5], Y. L. Chen[6], F. Iga[7], John Singleton[8], Y. Matsuda[2]*, Lu Li[1]*

In metals, orbital motions of conduction electrons on the Fermi surface are quantized in magnetic fields, which is manifested by quantum oscillations in electrical resistivity. This Landau quantization is generally absent in insulators. Here, we report a notable exception in an insulator—ytterbium dodecaboride (YbB_{12}). The resistivity of YbB_{12}, which is of a much larger magnitude than the resistivity in metals, exhibits distinct quantum oscillations. These unconventional oscillations arise from the insulating bulk, even though the temperature dependence of the oscillation amplitude follows the conventional Fermi liquid theory of metals with a large effective mass. Quantum oscillations in the magnetic torque are also observed, albeit with a lighter effective mass.

I n Kondo insulators, the hybridization between itinerant and localized electrons opens an insulating gap, and consequently, their resistivity diverges at low temperature (1, 2). Recently, there has been a lively debate about the nature of the ground state of Kondo insulator samarium hexaboride (SmB_6) in intense magnetic fields. Although mixed-valence SmB_6 is a good insulator (its resistance increases by five orders of magnitude when cooled down to 300 mK from room temperature), Landau-level (LL) quantization still occurs, and clear quantum oscillations are observed in its magnetization [the de Haas–van Alphen (dHvA) effect] (3, 4). The origin and interpretation of the dHvA oscillations in SmB_6 have been highly controversial, owing to a number of peculiar features. First, the oscillations are observed only in magnetization and not in electrical resistivity [the Shubnikov–de Haas (SdH) effect]. Second, unlike the heavy carriers revealed by the thermoelectric studies (5), oscillations appear to arise from quasiparticles with a very light effective mass ($m \ll m_e$, where m_e is the free electron mass) (3). Third, in floating zone–grown SmB_6 samples, the dHvA signal exhibits a striking deviation from the standard Lifshitz-Kosevich (LK) formula in Fermi-liquid theory (4). These observations point to either a topologically protected surface state (3) or the presence of an unconventional Fermi surface in an insulator (4). A number of intriguing physical origins have been proposed, including exciton-based magnetic breakdown (6, 7), Majorana-type charge-neutral Fermi surfaces (8), a failed superconducting ground state (9), and spinon Fermi surfaces (10, 11). A key to solving the most fundamental problem, the existence of "a Fermi surface in an insulator," lies in clarifying whether quantum oscillations—in particular, in charge transport—are observable in another insulating system.

Here, we present quantum oscillation studies of ytterbium dodecaboride (YbB_{12}), another cubic-structured rare-earth intermetallic compound. YbB_{12} has long been known as a mixed-valence Kondo insulator (12–14). It behaves as a monovalent metal with localized magnetic moments at room temperature, whereas a nonmagnetic insulating ground state develops at low temperatures. The opening of a narrow energy gap of 10 to 15 meV at the Fermi level has been confirmed with many experiments (15–17) and is attributed to the hybridization between the itinerant $5d$ and the localized $4f$ electrons. The mean valence of Yb ions in YbB_{12} is +2.9 (18), close to $4f^{13}$ (+3) configuration. Therefore, the f electrons are mostly localized, and the crystalline electric field (CEF) ground state is well defined. By contrast, because the mean valence of Sm ions in SmB_6 is +2.6 (19), f electrons are more itinerant, and the CEF scheme is not well defined. Therefore, the electronic structure of YbB_{12} is much simpler than that of SmB_6. Furthermore, early calculations in YbB_{12} predicted the existence of topological surface states owing to mirror-symmetry protection (20).

YbB_{12} single crystals are grown in a floating-zone furnace [(21), section 1]. Using the experimental setup shown in Fig. 1A, magnetic torque and magnetoresistance (MR) are measured up to 45 T simultaneously [(21), section 2]. The temperature dependence of the resistivity (Fig. 1B) confirms an increase of five orders of magnitude from room temperature to 50 mK. The resistivity has a weak temperature dependence below 2.2 K, resem-

bling the resistive "plateau" well known in SmB_6 at temperature (T) < 3.5 K (22). This "plateau" is an indication of the existence of extended in-gap states. Fitting with the thermal activation model of resistivity, $\rho(T) = \rho_0 \exp(\Delta/2k_BT)$, where k_B is the Boltzmann constant, reveals a two-gap feature with the gap width 12.5 meV (20 K < T < 40 K) and 4.7 meV (6 K < T < 12.5 K), respectively (Fig. 1B, inset), which is consistent with previous transport results (23). Upon applying the magnetic field, the negative slope of the $\rho(T)$ curve is preserved up to 45 T, with no hints of metallic behavior (Fig. 1C), indicating that the ground state is still gapped (fig. S5).

The field dependence of the magnetic torque in the insulating state of YbB_{12} is shown in Fig. 1D. We observed a step increase at 20 T followed by a decrease at 28 T. These features are weak metamagnetic transitions and/or crossovers that could potentially be related to the predicted field-induced staggered magnetism in Kondo insulators (24). Above ~37.5 T, the dHvA oscillations are clearly resolved (Fig. 1D). The dHvA oscillations appear well below the insulator-metal (I-M) transition field in our YbB_{12} samples, which was determined by means of pulsed field studies to be 45.3 to 47.0 T [(21), sections 4 and 5]. Fast Fourier transform (FFT) on the $\phi = 11.3°$ torque curve gives a dHvA frequency of $F = 720$ T (Fig. 1D, inset).

In Fig. 2A, the MR data at $\phi = 27.7°$ is plotted between 11.5 and 45 T. Given the zero-field resistivity $\rho(0) = 4.67$ ohm · cm of this sample at 350 mK, a significant negative MR {$[\rho(H) - \rho(0)]/\rho(0)$} of –95.9% is achieved at 45 T (a detailed angular dependence of MR is shown in fig. S3). The negative MR is a hallmark of Kondo insulators that results from field suppression of the hybridization gap (25–28). The negative MR in YbB_{12} is much larger than that in SmB_6 (29, 30). This is probably a consequence of the larger effective Landé g-factor in YbB_{12}, which increases the influence of the magnetic field (17, 28). As the magnetic field (H) increases, MR displays wiggle-like features at around 16 and 28 T. These wiggles do not arise from quantum oscillations because their positions are obviously temperature dependent (fig. S7); instead, they are likely to be field-induced transitions or crossovers. The feature at 28 T is probably linked to the kink feature in the magnetic torque [(21), section 6].

The most striking result in Fig. 2A is the oscillations that appear in the MR under strong magnetic fields. From 40.8 up to 45 T, two valleys and one peak in total can be clearly observed (Fig. 2A, top inset). The FFT on the MR oscillations in this field regime yields a clear frequency peak at $F = 913$ T (Fig. 2A, bottom inset). With the magnetic field direction close to the crystal axes, up to four oscillation periods can be seen (Fig. 2B). The overall SdH patterns are almost identical for $\phi = 11.3°$ and $\phi = 78.4°$, whereas there is a small valley position shift between $\phi = 18.3°$ and $\phi = 70.5°$. This suggests an axis of symmetry along [101] direction for the SdH oscillations, which is consistent with the cubic structure of YbB_{12} crystal (fig. S10). The valleys in $d\rho/dH$ in Fig. 2B being approximately uniformly

[1]Department of Physics, University of Michigan, Ann Arbor, MI 48109, USA. [2]Department of Physics, Kyoto University, Kyoto 606-8502, Japan. [3]Faculty of Applied Science, Université Chrétienne Bilingue du Congo, Beni, North-Kivu, Democratic Republic of Congo. [4]Japan Synchrotron Radiation Research Institute, Sayo, Hyogo 679-5198, Japan. [5]National Laboratory of Solid State Microstructures, Nanjing University, Nanjing 210093, China. [6]Department of Physics, Clarendon Laboratory, University of Oxford, Oxford OX1 3PU, UK. [7]College of Science, Ibaraki University, Mito 310-8512, Japan. [8]National High Magnetic Field Laboratory, Los Alamos National Laboratory, Los Alamos, NM 87545, USA.
*Corresponding author. Email: luli@umich.edu (L.L.); matsuda@scphys.kyoto-u.ac.jp (Y.M.)

spaced as a function of $1/H$ provides strong evidence that the SdH oscillations have a single dominating frequency. These overall patterns of the SdH oscillations, as well as those of the dHvA oscillations, are well reproduced between different YbB$_{12}$ samples [(21), section 3].

The observation of the SdH oscillations is reinforced by the temperature dependence of oscillation amplitudes. The evolution of the high-field wiggle features in both MR and torque data shows the typical behavior of quantum oscillations, with temperature-independent positions of the dominant peaks and valleys within the uncertainty and an attenuated amplitude from base temperature up to 1.5 K (figs. S7 and S8). The temperature-dependent amplitudes of normalized oscillatory torque (Fig. 3A) and oscillatory MR (Fig. 3, B and C) are fitted by using the conventional LK formula (31). The fittings are reasonably good down to 60 mK, indicating that the LK expression, based on the Fermi liquid framework, appears to be valid in the Kondo insulator YbB$_{12}$. The agreement with the LK description confirms that the features we resolve are quantum oscillations rather than successive field-induced Lifshitz transitions.

The SdH oscillations are much more suppressed at higher temperatures as compared with dHvA oscillations at the same angle (Fig. 3, A and B), revealing a heavier effective mass in the electrical transport channel. The effective masses of the quasiparticles estimated from the dHvA and SdH

oscillations at the same tilt angle are ~6.6 m_e and 14.6 m_e, respectively. Therefore, it is unlikely that both types of oscillations originate from the same band. The SdH and dHvA frequencies have different angle dependences (Fig. 4). The dHvA frequencies F can be tracked with a two-dimensional (2D) Fermi surface model ($F \propto \frac{1}{\cos\theta}$) with the in-plane cross section area $A_{[001]} = 6.67$ nm^{-2} (Fig. 4, solid line). Given the lack of dHvA oscillations observed above $\simeq 20°$ (fig. S9), this inverse sinusoidal dependence can be explained by either a 2D Fermi cylinder or a heavily elongated 3D Fermi pocket. On the other hand, the angular dependence of the SdH frequencies displays a clearly nonmonotonic behavior: A frequency maximum appears at $\theta \sim 15°$ to $20°$ from the crystal axes, resulting in an "M"-shape with a local dip at $H \parallel [100]$ and a fast decrease in the frequency beyond the maximum. The 2D Fermi surface model apparently cannot describe this behavior. Our attempt to model the SdH frequencies (Fig. 4, dashed lines, and figs. S1 and S10) points to hyperbolic "neck" orbits [(21), section 8].

The amplitude of the quantum oscillations is determined by a combination of temperature, band curvature, Dingle, and spin factors. Assuming Dingle and spin factors do not depend on the band, the oscillation amplitude of the light band with the 2D character should be much larger than that of the heavy band with the 3D character. Because the observed SdH oscillations arise from

a relatively heavy band ($m^* \approx 15\ m_e$), it is highly unusual that the oscillations observed in the dHvA effect, which detects the orbits from a much lighter band ($m^* \approx 6.6\ m_e$), are not present in the SdH effect. We discuss in section 11 of (21) the possible origins of the dHvA oscillations, based on either surface state (32), charge-neutral Fermi surface (10), or a minority phase. Further, on the basis of the symmetry analysis and other tests in a even stronger magnetic field, the bulk SdH oscillations do not arise from metallic impurity phases [(21), sections 7, 9, and 10] or from a minority portion of sample, which has a lower I-M transition field [(21), sections 4 and 5].

There are several notable features in the SdH oscillations that we observed. The effective masses obtained from LK fittings are large, which is in agreement with the nature of a Kondo insulator in which strong electron correlations make the quasiparticles heavy. Even in the insulating state, a finite electronic specific heat coefficient γ is observed in YbB$_{12}$ (33). Assuming a spherical Fermi surface with $k_F \sim 0.156$ Å^{-1} ($F = 800$ T) and effective mass $m^* = 15\ m_e$ obtained from the SdH oscillations, the value of γ is calculated to be 7.6 mJ/mol K^2, comparable with the observed value of $\gamma \sim 8$ mJ/mol K^2 at 39 T (33). The background resistivity ρ still has a magnitude of more than 100 milliohm · cm above 40 T, which is well beyond that of normal metals (34). If we estimate the mean free path ℓ by considering a spherical

Fig. 1. Electrical transport and magnetic torque measurements in YbB$_{12}$. (**A**) Sketch of the experimental setup (21) and the definition of tilt angle ϕ with respect to the magnetic field. (Inset) Photograph of a YbB$_{12}$ single crystal (sample N2) mounted onto a cantilever beam magnetometer, with four gold wires attached to the crystallographic (001) surface for the transport measurement. (**B**) Resistivity of two YbB$_{12}$ single crystals plotted as a function of temperature. (Inset) The Arrhenius plot, lnρ versus $1/T$. According to the thermal activation model, the slope of the Arrhenius plot equals $\Delta/2k_B$, where Δ is the bandgap width and k_B is the Boltzmann constant. Linear fitting in two different temperature ranges, $20 < T < 40$ K and $6 < T < 2.5$ K, yields two characteristic gap widths, 12.5 and 4.7 meV, respectively. (**C**) Resistivity of YbB$_{12}$ sample N2 under different magnetic fields from 0 to 45 T, plotted against temperature. Open and solid symbols are data taken in ^{3}He cryostat at $\phi = 7.4°$ and in dilution fridge at $\phi = 8.5°$, respectively. Solid lines are guides to the eye. (**D**) Magnetic torque in YbB$_{12}$ measured at $T = 350$ mK and at two different tile angles, $\phi = -6.8°$ and $\phi = 11.3°$. Both exhibit strong quantum oscillations under high magnetic fields. The amplitude of the oscillatory part of magnetic torque at $\phi = 11.3°$ is ~6 × 10^{-8} N · m at the highest field, corresponding to an effective transverse magnetization of ~1.4 × 10^{-9} A · m^2 (1.51 × 10^{14} μ_B). (Inset) FFT on the magnetic torque signal with $\phi = 11.3°$ reveals a major peak at $F = 720$ T and its harmonics.
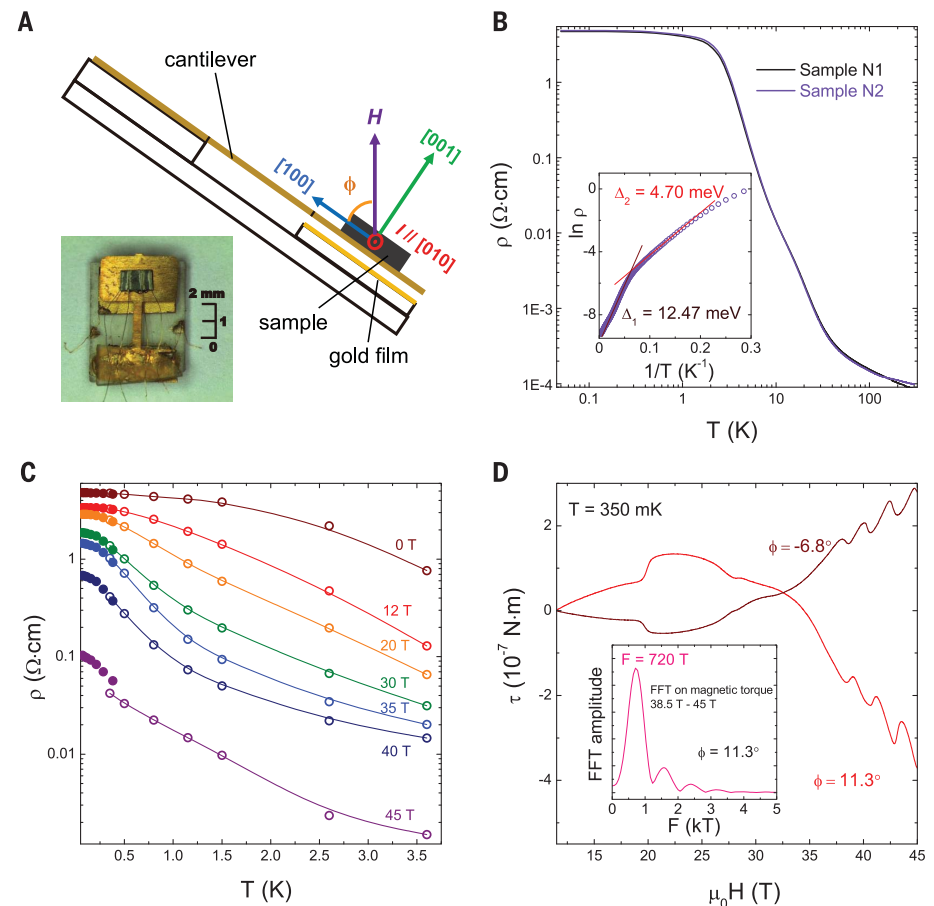
Fig. 2. Resistivity and electrical oscillations in intense magnetic fields in YbB$_{12}$. (**A**) Resistivity of sample N2 as a function of magnetic field measured up to 45 T taken at T = 350 mK at a tilt angle ϕ = 27.7°. Quantum oscillations are clearly observed at high magnetic field beyond 40.8 T. The extrema are marked by arrows. (Top inset) First magnetic field derivative of resistance has two prominent valleys and one peak. (Bottom inset) FFT on the magneto-resistance data presented between $\mu_0 H$ = 40.5 T and 45 T. A single peak frequency of F = 913 T is resolved. (**B**) Field derivative of sample resistivity at four different tilt angles. Dotted lines mark the approximately evenly spaced valleys of SdH oscillation. Three to four periods in total can be observed, depending on the field orientation. The oscillation pattern at ϕ is repeated at $90° - \phi$, which is consistent with the cubic symmetry of crystal structure.
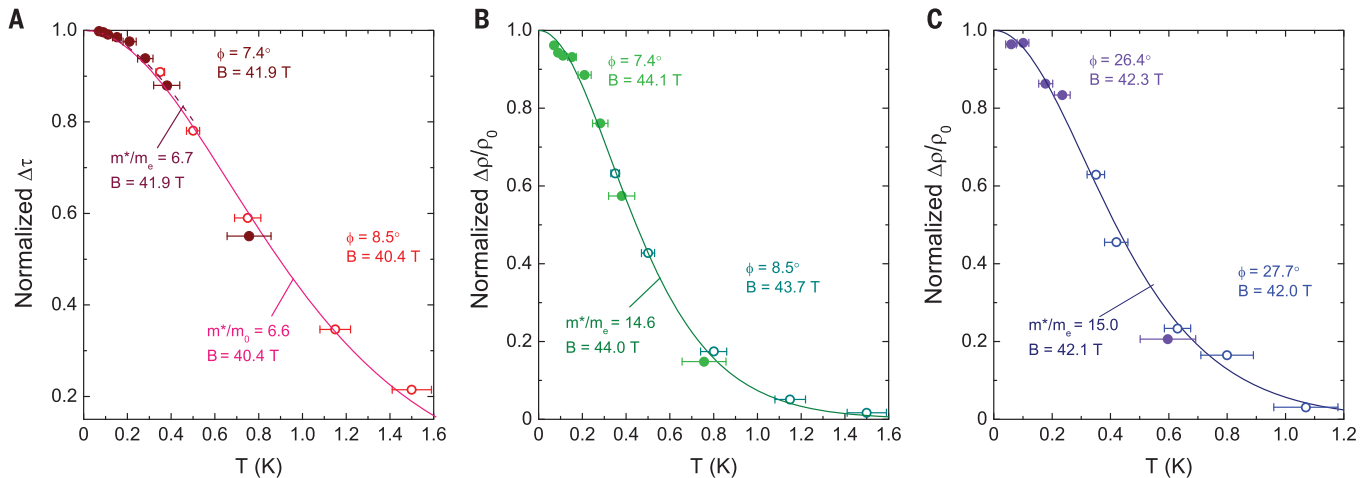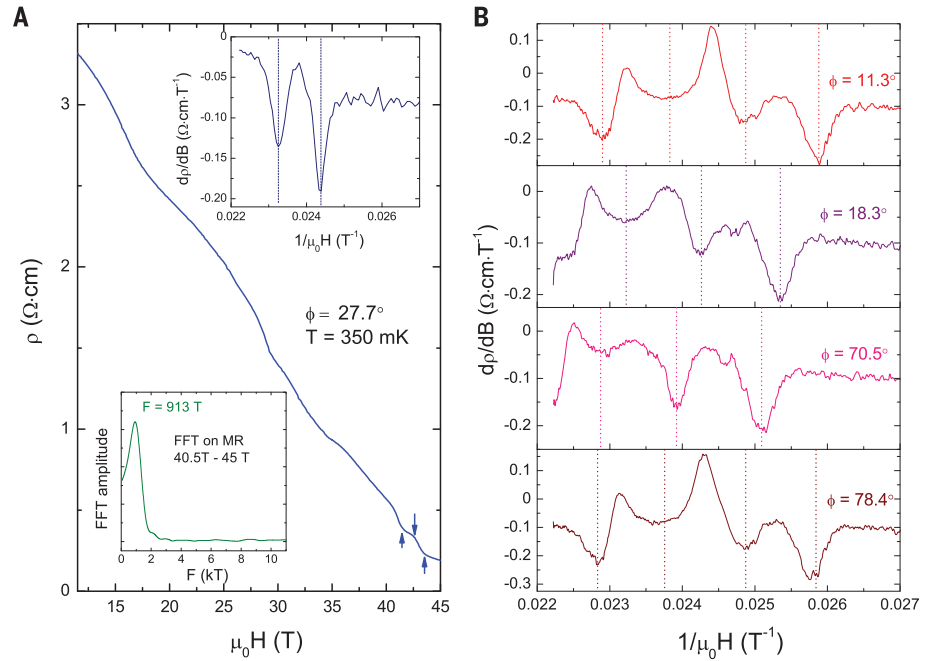
Fig. 3. Effective mass fitting on dHvA and SdH oscillations in YbB$_{12}$. (**A**) Normalized dHvA oscillation amplitude $\Delta\tau$ as a function of temperature. Open circles and solid circles are the data taken in ^{3}He cryostat at ϕ = 8.5° and in portable dilution fridge at ϕ = 7.4°, respectively. The LK model fitting by using parameters m^* = 6.6 m_e, B = 40.4 T is indicated with a solid line based on the ^{3}He cryostat data. In comparison, the LK fitting based on the portable dilution fridge data gives m^* = 6.7 m_e, B = 41.9 T, which is indicated with the dashed line. (**B** and **C**) Temperature dependence of normalized SdH amplitude $\Delta\rho/\rho_0$. (B) is taken at the same tilt angle as in (A), and (C) is taken at a tilt angle close to that in Fig. 2A. Open and solid symbols are data measured in portable ^{3}He cryostat and dilution fridge, respectively. Here, ρ_0 is the zero-field resistivity at corresponding temperatures. Solid lines are fittings based on the LK formula, with parameters shown in each panel. According to the fittings, SdH effective mass exhibits a weak anisotropy between $\phi \simeq 8°$ [(B), m^* = 14.6 m_e] and $\phi \simeq 27°$ and [(C), m^* = 15.0 m_e]. In (A) to (C), the quantum oscillation amplitudes (raw data are shown in fig. S8) are taken as the averaged value of an adjacent peak and valley obtained after subtracting a polynomial background from the raw data, and the effective magnetic field for each data set is an inverse average of the peak and valley positions. [Details of the background subtraction and the determination of the B parameters in the LK fittings are presented in (21), section 6.] The error bars on the temperature are estimated based on the MR effect on the ruthenium oxide thermometer above 11.4 K.

Fermi surface with m^* = 15 m_e and setting ρ = 0.4 ohm · cm (Fig. 2A), we will obtain an un-physically short mean free path, $\ell \sim 0.01$ nm.

Unconventional quantum oscillations have been proposed in insulators with hybridization gaps (6–11, 35, 36). However, our discovery of quantum oscillations in charge transport cannot be effectively interpreted by the theories that either invoke charge-neutral quasiparticles (7–9) or associate the oscillations with the grand canonical potential (6). All these theories of exotic quantum oscillations predict that in a gapped system, the temperature dependence of the oscillation amplitude deviates from the conventional LK-formula at certain elevated temperatures. By contrast, our observations show that in YbB$_{12}$, the LK formu-la works from T = 1.5 K (0.13 meV) down to T = 60 mK (0.0052 meV), a range of energy lower than both the hybridization gap width and the cyclotron energy of charge carriers at a field of $\simeq$40 T [(21), section 11]. Recent theories suggest that an emergent neutral Fermi sea can exist in a mixed-valence gapped system and exhibit both dHvA and SdH oscillations (10, 11), which may
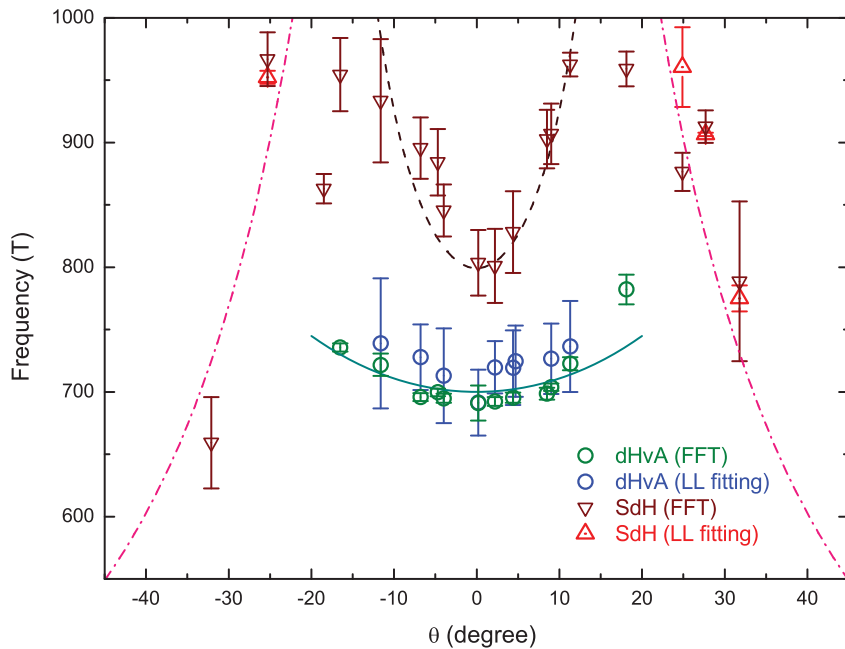
Fig. 4. Angular dependence of quantum oscillation frequencies. The frequencies of the quantum oscillations appearing at high field in YbB$_{12}$. Magnetic field H is rotated in a plane perpendicular to the current direction, and the effective tilt angle θ is defined as the angle between H and the equivalent crystal axes [001]/[100] in a cubic structure. Circles are dHvA frequencies obtained from FFT (green) and the slope of a linear fitting of the LL index versus inverse magnetic field (blue). The solid line is a calculation by using 2D Fermi surface model: $F = F_0/\cos\theta$ with $F_0 = 700$ T. Up triangles (red) and down triangles (brown) are SdH frequencies acquired from the FFT and from the linear fitting of the LL index plot, respectively. The dashed line is the fitting by a hyperboloid model representing a Fermi surface neck region with the principal axis along the [001] direction, whereas the dash-dot lines are simulation for the high-angle data points by using an oblate spheroid model with the principal axis along [001] direction. The detailed parameters in these models are provided in (21), section 8. The error bars come from the difference between different sampling windows for the FFT results and from the linear fitting error for the LL analysis.

shed light on the exotic SdH oscillations we resolved, although a deviation from LK formula is still required in this scenario. A proper theory is yet to be established to describe the quantum oscillations observed in YbB$_{12}$ under a high magnetic field.

REFERENCES AND NOTES

1. H. Tsunetsugu, M. Sigrist, K. Ueda, *Rev. Mod. Phys.* **69**, 809–864 (1997).
2. P. S. Riseborough, *Adv. Phys.* **49**, 257–320 (2000).
3. G. Li *et al.*, *Science* **346**, 1208–1212 (2014).
4. B. S. Tan *et al.*, *Science* **349**, 287–290 (2015).
5. Y. Luo, H. Chen, J. Dai, Z. Xu, J. D. Thompson, *Phys. Rev. B* **91**, 075130 (2015).
6. J. Knolle, N. R. Cooper, *Phys. Rev. Lett.* **115**, 146401 (2015).
7. J. Knolle, N. R. Cooper, *Phys. Rev. Lett.* **118**, 096604 (2017).
8. G. Baskaran, Majorana arXiv:1507.03477 [cond-mat.str-el] (2015).
9. O. Erten, P.-Y. Chang, P. Coleman, A. M. Tsvelik, *Phys. Rev. Lett.* **119**, 057603 (2017).
10. D. Chowdhury, I. Sodemann, T. Senthil, *Nat. Commun.* **9**, 1766 (2018).
11. I. Sodemann, D. Chowdhury, T. Senthil, *Phys. Rev. B* **97**, 045152 (2018).
12. M. Kasaya, F. Iga, K. Negishi, S. Nakai, T. Kasuya, *J. Magn. Magn. Mater.* **31-34**, 437–438 (1983).
13. M. Kasaya, F. Iga, M. Takigawa, T. Kasuya, *J. Magn. Magn. Mater.* **47-48**, 429–435 (1985).
14. T. Kasuya, *Europhys. Lett.* **26**, 277–281 (1994).
15. J.-M. Mignot *et al.*, *Phys. Rev. Lett.* **94**, 247204 (2005).
16. M. Okawa *et al.*, *Phys. Rev. B* **92**, 161108 (2015).
17. T. T. Terashima *et al.*, *J. Phys. Soc. Jpn.* **86**, 054710 (2017).
18. J. Yamaguchi *et al.*, *Phys. Rev. B* **79**, 125121 (2009).
19. Y. Utsumi *et al.*, *Phys. Rev. B* **96**, 155130 (2017).
20. H. Weng, J. Zhao, Z. Wang, Z. Fang, X. Dai, *Phys. Rev. Lett.* **112**, 016403 (2014).
21. Materials, methods, and additional data are available as supplementary materials.
22. J. C. Cooley, M. C. Aronson, Z. Fisk, P. C. Canfield, *Phys. Rev. Lett.* **74**, 1629–1632 (1995).
23. F. Iga, N. Shimizu, T. Takabatake, *J. Magn. Magn. Mater.* **177-181**, 337–338 (1998).
24. K. S. D. Beach, P. A. Lee, P. Monthoux, *Phys. Rev. Lett.* **92**, 026401 (2004).
25. K. Sugiyama, F. Iga, M. Kasaya, T. Kasuya, M. Date, *J. Phys. Soc. Jpn.* **57**, 3946–3953 (1988).
26. T. Takabatake *et al.*, *Phys. Rev. B Condens. Matter* **45**, 5740–5743 (1992).
27. G. S. Boebinger, A. Passner, P. C. Canfield, Z. Fisk, *Physica B* **211**, 227–229 (1995).
28. J. C. Cooley *et al.*, *Phys. Rev. B Condens. Matter* **52**, 7322–7327 (1995).
29. J. C. Cooley *et al.*, *J. Supercond.* **12**, 171–173 (1999).
30. S. Wolgast *et al.*, *Phys. Rev. B* **92**, 115110 (2015).
31. D. Shoenberg, *Magnetic Oscillations in Metals* (Cambridge Univ. Press, 2009).
32. K. Hagiwara *et al.*, *Nat. Commun.* **7**, 12690 (2016).
33. T. Terashima *et al.*, *Phys. Rev. Lett.* **120**, 257206 (2018).
34. M. Gurvitch, *Phys. Rev. B* **24**, 7404–7407 (1981).
35. L. Zhang, X.-Y. Song, F. Wang, *Phys. Rev. Lett.* **116**, 046404 (2016).
36. H. K. Pal, F. Piéchon, J.-N. Fuchs, M. Goerbig, G. Montambaux, *Phys. Rev. B* **94**, 125140 (2016).

Science

Quantum oscillations of electrical resistivity in an insulator

Z. Xiang, Y. Kasahara, T. Asaba, B. Lawson, C. Tinsman, Lu Chen, K. Sugimoto, S. Kawaguchi, Y. Sato, G. Li, S. Yao, Y. L. Chen, F. Iga, John Singleton, Y. Matsuda and Lu Li

Insulator or a metal?

When a metal is cooled to low temperatures and placed in an external magnetic field, its resistivity may oscillate as the magnitude of the field is varied. Seeing these so-called quantum oscillations in an insulating material would be very unusual. Xiang *et al.* report such findings in the insulator ytterbium dodecaboride (YbB_{12}) (see the Perspective by Ong). In addition to oscillations in resistivity, the authors observed oscillations in the magnetic torque. The results present a challenge to theories that aim to explain the insulating state of YbB_{12}.

Science, this issue p. 65; see also p. 32

ARTICLE TOOLS	http://science.sciencemag.org/content/362/6410/65
SUPPLEMENTARY MATERIALS	http://science.sciencemag.org/content/suppl/2018/08/29/science.aap9607.DC1
RELATED CONTENT	http://science.sciencemag.org/content/sci/362/6410/32.full
REFERENCES	This article cites 47 articles, 2 of which you can access for free http://science.sciencemag.org/content/362/6410/65#BIBL
PERMISSIONS	http://www.sciencemag.org/help/reprints-and-permissions

Use of this article is subject to the Terms of Service